

This is an Open Access document downloaded from ORCA, Cardiff University's institutional repository: <https://orca.cardiff.ac.uk/id/eprint/109195/>

This is the author's version of a work that was submitted to / accepted for publication.

Citation for final published version:

Hosking, L. J. . , Thomas, H. R. and Sedighi, M. 2018. A dual porosity model of high pressure gas flow for geoenery applications. *Canadian Geotechnical Journal* 55 (6) , pp. 839-851. 10.1139/cgj-2016-0532

Publishers page: <http://dx.doi.org/10.1139/cgj-2016-0532>

Please note:

Changes made as a result of publishing processes such as copy-editing, formatting and page numbers may not be reflected in this version. For the definitive version of this publication, please refer to the published source. You are advised to consult the publisher's version if you wish to cite this paper.

This version is being made available in accordance with publisher policies. See <http://orca.cf.ac.uk/policies.html> for usage policies. Copyright and moral rights for publications made available in ORCA are retained by the copyright holders.



A dual porosity model of high pressure gas flow for geoenergy applications

Hosking, L.J.¹, Thomas, H.R.¹, and Sedighi, M.²

¹*Geoenvironmental Research Centre, Cardiff School of Engineering, Cardiff University, The Queen's Buildings, Newport Road, Cardiff, CF24 3AA, UK*

²*School of Mechanical, Aerospace and Civil Engineering, The University of Manchester, Manchester, M1 3PL, UK*

Abstract

This paper presents the development of a dual porosity numerical model of multiphase, multicomponent chemical/gas transport using a coupled thermal, hydraulic, chemical and mechanical formulation. Appropriate relationships are used to describe the transport properties of non-ideal, reactive gas mixtures at high pressure, enabling the study of geoenergy applications such as geological carbon sequestration. Theoretical descriptions of the key transport processes are based on a dual porosity approach considering the fracture network and porous matrix as distinct continua over the domain. Flow between the pore regions is handled using mass exchange terms and the model includes equilibrium and kinetically-controlled chemical reactions. A numerical solution is obtained with a finite element and finite difference approach and verification of the model is pursued to build confidence in the accuracy of the implementation of the dual porosity governing equations. In the course of these tests, the time splitting approach used to couple the transport, mass exchange and chemical reaction modules is shown to have been successfully applied. It is claimed that the modelling platform developed provides an advanced tool for the study of high pressure gas transport, storage and displacement for geoenergy applications involving multiphase, multicomponent chemical/gas transport in dual porosity media, such as geological carbon sequestration.

Keywords: dual porosity, gas flow, high pressure, carbon sequestration, geoenergy

¹ Corresponding author: Dr Lee J. Hosking
Geoenvironmental Research Centre, Cardiff School of Engineering, Cardiff University, Queen's Buildings, The Parade, CF24 3AA, Cardiff, UK, Email: HoskingL@cardiff.ac.uk, Tel: 02920 870497

24 **Introduction**

25 Climate change poses a great threat to the environment and society, yet there is a growing global demand
26 for energy and energy security is a political priority. Geoenergy technologies are prominent in the
27 strategies for climate change mitigation and adaptation developed as a collective response to these
28 issues. Geological carbon sequestration, for example, is intended to facilitate the decarbonisation of
29 reliable fossil fuel power plants by isolating carbon dioxide emissions in suitable deep rock formations
30 (Scott, Gilfillan et al. 2013). Other examples include enhanced hydrocarbon recovery, the exploration
31 of unconventional gas, and the deep geological disposal of nuclear waste. It is therefore important from
32 an engineering perspective to examine the complex, coupled phenomena governing the transport,
33 storage and displacement of multiphase, multicomponent chemicals and gas in the deep
34 geoenvironment. This study addresses the development of a numerical model for this purpose.

35 Fractures and discontinuities are commonly important features in geological formations and can have a
36 significant bearing on the water and gas flows and reactive chemical transport. They effectively divide
37 a geomaterial into two distinct porosities, namely, the fracture network and the porous matrix blocks
38 (Bear 1993). An understanding of the physical and chemical processes involved in multiphase flow in
39 each of these pore regions is important for a rigorous prediction of the phenomena arising in the
40 geoenergy applications mentioned above. Of particular interest are the differences in the fluid transport
41 and displacement behaviour, which may depend strongly on the inter-porosity flows and various
42 physical and chemical interactions between the solid, liquid and gas phases.

43 Several established modelling techniques are available to express the heterogeneous pore structure of a
44 dual porosity geomaterial in a form more amenable to numerical treatment. In broad terms, these may
45 be categorised as: i) discrete fracture network (DFN) models, ii) equivalent continuum models, and iii)
46 dual (or higher) porosity models (Therrien and Sudicky 1996). The selection of the most appropriate
47 type of model depends on the problem scale/conditions, the available input data, the type of output data
48 required, and the available computational resources (Bear 1993, Samardzioska and Popov 2005).

49 DFN models can provide a theoretically rigorous interpretation of a fractured rock, since an attempt is
50 made to explicitly model the flow in each and every hydraulically active fracture. They are attractive

51 provided these fractures can be identified and included within the modelling framework without
52 excessive costs in terms of input data and computation time. Simulation using a DFN model inherently
53 becomes more challenging as the problem scale increases, especially given the complexity of most
54 naturally fractured reservoirs (Samardzioska and Popov 2005, Singhal and Gupta 2010).

55 Equivalent continuum models provide a simpler alternative in which the dual porosity geomaterial is
56 described as a single homogenous medium, thereby reducing the input data requirements, theoretical
57 complexity, and computational cost compared to DFN models. They are suitable provided the
58 homogenisation process adopted can accurately capture the bulk properties of the geomaterial. In
59 practical terms this requires a dense, highly interconnected fracture network to ensure that the flows in
60 the fracture and matrix pore regions remain near equilibrium with each other (Berkowitz 2002). This
61 implies that the accuracy of equivalent continuum models reduces as the partition between the fracture
62 and matrix flows becomes more apparent.

63 If there is an appreciable partition between the fracture and matrix flows, it is more appropriate to
64 employ a dual porosity model where a fracture continuum interacts with a matrix continuum. To reflect
65 the material properties of most fractured rocks, it is generally true that the fracture continuum provides
66 the majority of the flow capacity and the matrix continuum provides the majority of the storage capacity.
67 In other words, the fracture continuum is more highly conductive with a lower porosity and the matrix
68 continuum is poorly (or non-) conductive with a higher porosity (Bear 1993, Xu and Pruess 2001).
69 Provided representative properties can be assigned to the continua and the inter-porosity flow
70 interactions can be accurately theorised, a dual porosity model can capture the salient transport
71 behaviour of both fractured rocks (e.g. Bai, Elsworth et al. 1993, Xu, Sonnenthal et al. 2001, Di Donato
72 and Blunt 2004) and structured soils (e.g. Ray, Ellsworth et al. 1997, Schwartz, Juo et al. 2000).

73 Figure 1 shows three types of dual (or triple) porosity models that can be formulated to describe the
74 reactive transport processes in highly fractured geomaterials (e.g. coal). A conventional dual porosity
75 model, depicted in Figure 1a, assumes that the matrix porosity contains immobile fluids and chemicals
76 so that there is only a single permeability, i.e. the fracture permeability. In this manner, the matrix
77 porosity acts mainly as a sink/source to the mobile fluids and chemicals in the fractures. If the mobility

78 of the fluids and chemicals in the matrix porosity is considered, the result is the dual porosity, dual
79 permeability model shown in Figure 1b. Finally, the triple porosity model illustrated in Figure 1c may
80 be more appropriate in materials with a multi-modal matrix pore size distribution (e.g. macro-/micro-
81 pores), as found in some coals (Clarkson and Bustin 1999, Shi and Durucan 2005).

82 This paper describes an advanced theoretical formulation for multiphase, multicomponent reactive
83 chemical and gas transport in fractured geomaterials, including non-ideal gas behaviour. The dual
84 porosity, dual permeability approach is preferred since it has been quite widely and successfully applied
85 to this class of problems, for example in the study of coal (e.g. King, Ertekin et al. 1986, Clarkson and
86 Bustin 1999, Shi and Durucan 2005, Ozdemir 2009, Wu, Liu et al. 2010, Thararoop, Karpyn et al. 2012),
87 which is particularly relevant to the present work. Moreover, from the discussion given above, dual
88 porosity models are seen to offer an attractive balance of accuracy versus practicality, requiring neither
89 large input data sets nor excessive computational effort as the problem scale increases. Theoretical
90 features relating to the coupled hydraulic, chemical, gas and mechanical behaviour have been included
91 in the formulation presented. An example is the swelling of coal in response to gas adsorption, which
92 can have a considerable feedback effect on the porosity and permeability (Clarkson and Bustin 2010).

93 The theoretical formulation has been implemented in an existing coupled thermal, hydraulic, chemical
94 and mechanical (THCM) model, COMPASS, developed incrementally at the Geoenvironmental
95 Research Centre by Thomas and co-workers (Thomas and He 1998, Cleall, Seetharam et al. 2007,
96 Seetharam, Thomas et al. 2007, Thomas, Sedighi et al. 2012, Sedighi, Thomas et al. 2016). COMPASS
97 has a background of high performance simulations of three-dimensional multiphase, multicomponent
98 reactive transport in single porosity geomaterials, based on a theoretical formulation that can be
99 described as a mechanistic approach. Geochemical reactions between components in the liquid, gas and
100 solid phases are considered via the coupling of COMPASS to the geochemical model, PHREEQC
101 (version 2) (Parkhurst and Appelo 1999), with the COMPASS-PHREEQC platform having been applied
102 to study a range of problems including the performance of engineered barriers for the deep geological
103 disposal of nuclear waste. This paper presents recent developments that extend the existing capabilities
104 towards the aforementioned areas of geoenergy engineering, particularly carbon sequestration, achieved

105 principally through the introduction of the dual porosity framework and the inclusion of non-ideal gas
106 behaviour (Hosking 2014). A series of benchmark tests have been performed on the new model to verify
107 the correctness of the numerical implementation, with the results of these tests also being presented in
108 this paper.

109 By incorporating the new developments into the pre-existing THCM framework of COMPASS, this
110 work has yielded an advanced model of high pressure gas transport, storage and displacement for
111 geoenergy applications involving multiphase, multicomponent chemical/gas transport in dual porosity
112 media. Beyond being a predictive tool, the mechanistic approach adopted allows for a detailed insight
113 into the underlying coupled processes that govern the overall system behaviour, as well as providing
114 flexibility for the continued development of the model.

115 **Dual porosity theoretical formulation**

116 The fracture network and porous matrix blocks are handled as distinct continua over the domain and
117 each flow variable has fracture and matrix values at every analysis point. This yields a system of
118 governing equations expressed in terms of six primary variables, namely, the pore water pressure in the
119 fractures () and matrix (), the concentrations of chemical components in the aqueous phase in
120 the fracture () and matrix (), and the concentrations of chemical components in the gas phase in
121 the fracture () and matrix (). The gas phase is thereby modelled by considering the coupled
122 behaviour of its constituent chemical components. Mechanical behaviour is not explicitly considered in
123 the present work, with the feedback of deformation instead considered implicitly using constitutive
124 relationships describing the evolution of porosity and permeability as effective stress and chemo-
125 mechanical conditions change.

126 Chemical flow through the continua is considered by advection, diffusion and dispersion mechanisms.
127 Darcy's law is used to describe the advective flow due to pressure and gravitational gradients and Fick's
128 law is used to describe molecular diffusion, with mechanical dispersion treated analogously to molecular
129 diffusion (Bear and Verruijt 1987). Sink/source terms are included to: i) handle equilibrium and
130 kinetically-controlled chemical reactions, and ii) define the mass exchange processes which couple the

131 flows in the fracture and matrix continua.

132 The governing equations for coupled thermal, hydraulic and aqueous chemical behaviour in unsaturated
133 soils have been covered in detail elsewhere (Thomas and He 1998, Cleall, Seetharam et al. 2007,
134 Thomas, Sedighi et al. 2012, Sedighi, Thomas et al. 2016). In addition, the governing equations for the
135 reactive transport of multicomponent gas in a single porosity unsaturated soil have been presented by
136 Masum (2012) and Sedighi et al. (2015), assuming ideal gas behaviour. Thus, the focus of this paper is
137 on presenting the governing equations and model development for water transfer and multicomponent
138 reactive chemical transport in dual porosity geomaterials. In addition, the theoretical aspects
139 implemented in the model in relation to non-ideal gas flow at high pressure are presented.

140 *General form of the governing equations*

141 Based on the principle of conservation of mass, the temporal derivative of the water content and
142 chemical accumulation is equal to the spatial gradient of the relevant fluxes. Sink/source terms are
143 included allowing for chemical reactions and mass exchange between the fracture and matrix continua.
144 The dual porosity governing equations for water transfer (equation (1)) and the reactive transport of the
145 dissolved or gaseous chemical component (equation (2)) are then given by:

$$\text{---} \tag{1}$$

$$\text{---} \tag{2}$$

146 where the subscript i is the phase identifier for chemical components and becomes d to denote dissolved
147 chemical components and g to denote gaseous chemical components. Similarly, the subscript j is the
148 continuum identifier and becomes f to denote the fracture network and m to denote the porous matrix.
149 The superscript k denotes the component number of the chemical and gas species present in the
150 multiphase, multicomponent system. Accordingly, $\frac{\partial}{\partial t} \left(\rho_{i,j} \right)$ if $i = d$ or $i = g$ if $i = g$, where
151 n_d and n_g are the number of dissolved and gas components, respectively. On the left hand side of
152 equations (1) and (2), the parameter $\theta_{i,j}$ is the volumetric water (if $i = d$) or gas (if $i = g$) content,
153 ρ_w is the density of liquid water, and $S_{i,j}$ is the sink/source term for the accumulation/generation of the

154 chemical component due to chemical reactions. The flux components are included on the right hand
 155 side of the governing equations, where \mathbf{v} represents the advective velocity, D_{eff} is the effective
 156 diffusion coefficient and α_p is the coefficient of mechanical dispersion. In the final terms, S_{12} and
 157 represent the sinks/sources for mass exchange between the continua, with $S_{12} > 0$ if $S_{12} < 0$ or $S_{12} = 0$ if
 158 .

159 The volumetric water or gas content, V_w , can be expressed in terms of the porosity and the degree of
 160 saturation, as:

$$(3)$$

161 where ϕ is the porosity and S_w is the degree of water or gas saturation. In the absence of water vapour,
 162 the volumetric liquid and gas contents, V_w and V_g , in a two phase system are bound by the
 163 relationship:

$$(4)$$

164 Application of Darcy's law yields the following expression for \mathbf{q} in equations (1) and (2) (Bear and
 165 Verruijt 1987):

$$(5)$$

166 where z is the elevation and K_{rg} , the unsaturated hydraulic or gas conductivity, can be expanded to
 167 give:

$$(6)$$

168 where k is the intrinsic permeability, $k_{r,g}$ is the phase relative permeability, and μ_g is the absolute
 169 phase viscosity.

170 In determining the bulk gas phase velocity, \mathbf{v}_g , the bulk gas pressure, i.e. p_g , can be expressed in
 171 terms of the sum of the concentrations of the chemical components in the gas phase using the non-ideal
 172 gas law, given by:

(7)

173 where β is the compressibility factor, i.e. the ratio of the actual molar volume to that predicted by the
174 ideal gas law, R is the universal gas constant, and T is the temperature.

175 The effective diffusion coefficient, D_{eff} , in equation (2) is derived from the free fluid diffusion
176 coefficient, D , to account for the tortuous diffusion paths in a porous medium. This relationship can
177 be written as (Cussler 1997):

(8)

178 where τ is the tortuosity factor.

179 Mechanical dispersion in the gas phase is considered negligible compared to diffusion since gas
180 diffusion coefficients are around four orders of magnitude greater than those of dissolved chemicals
181 (Cussler 1997). Hence, $D_{eff} \approx D$. Furthermore, Therrien and Sudicky (1996) reported that mechanical
182 dispersion of dissolved chemicals in rock matrix blocks is generally weak compared to diffusion and by
183 experience may also be neglected, giving $D_{eff} \approx D$.

184 ***Porosity and permeability***

185 It is important to clearly define how the porosity and permeability of the fracture and matrix continua
186 are assigned, since characterisation tests conventionally do not (or cannot) distinguish between the
187 different pore regions (Schwartz, Juo et al. 2000). With reference to Figure 2, the matrix continuum is
188 assigned the properties of the unaltered porous rock matrix, ignoring any minor splay fractures. The
189 properties in the local region of an open fracture are more complex since fractures are not necessarily
190 clear flow conduits. Open fractures can be partially or completely blocked by infilling minerals such as
191 carbonates, quartz and clays (Ward 2002), and the presence of a fracture may also give rise to a zone of
192 altered porous matrix surrounding the discontinuity. The extent of this zone is likely to be larger in softer
193 rocks, such as coal, compared to harder rocks, such as granite. In this work, an attempt has been made
194 to assign properties to the fracture continuum that represent those of the fracture ‘zone’ comprising open
195 fractures, mineral infillings and the altered porous matrix.

196 The fracture continuum porosity, ϕ_f , is the fraction of the total porosity associated with the fracture
 197 zone, expressed mathematically as (Gerke and van Genuchten 1993, Zheng and Samper 2015):

$$(9)$$

198 where $\phi_{f,loc}$ is the local fracture porosity given by the volume of the pores in the fracture zone divided by
 199 the total volume of the fracture zone, i.e. $\phi_{f,loc} = \frac{V_{pore}}{V_{fracture}}$. This becomes 1.0 in a clean fracture, but may be less
 200 due to mineral infillings and the presence of altered porous matrix surrounding the fracture. The
 201 parameter ω is the volumetric weighting factor, defined as the total volume of the fracture zone divided
 202 by the total volume, i.e. $\omega = \frac{V_{fracture}}{V_{total}}$ (Zheng and Samper 2015), analogous to the following expression
 203 if the matrix blocks have a more or less regular cubic geometry:

$$\phi_f = \frac{\omega \phi_{f,loc}}{\omega \phi_{f,loc} + (1 - \omega) \phi_m} \quad (10)$$

204 where a and b are the fracture aperture and matrix block half-width, respectively.

205 Equation (9) allows the matrix continuum porosity, ϕ_m , to be expressed in terms of the total porosity,
 206 ϕ , and ϕ_f , as:

$$(11)$$

207 Therefore, provided the values of ϕ , ϕ_f and ω can be measured or estimated, the distribution of the
 208 porosity can be defined. While the measurement of ϕ via experimental techniques (e.g. porosimetry)
 209 does not present a major challenge, it is more difficult to distinguish between the fracture and matrix
 210 values. Nonetheless, equation (10) may be applied to estimate ϕ_m , and there are some field and
 211 laboratory techniques available to estimate the fracture porosity, i.e. ϕ_f (Singhal and Gupta 2010).

212 Similarly, the total intrinsic permeability, k_{int} , can be readily measured in the laboratory via core flooding
 213 experiments. In order to distribute the observed permeability between the dual pore regions, it is useful
 214 to consider the wide body of literature supporting the notion that the fracture network permeability is
 215 typically several orders of magnitude greater than the porous matrix permeability (Tsang and Pruess
 216 1987, Bear 1993, Bandurraga and Bodvarsson 1999, Philip, Jennings et al. 2005). As an example, it is
 217 up to eight orders of magnitude greater in coal (Robertson 2005). It is therefore assumed that the total

218 permeability, k_{fr} , determined in a laboratory test belongs to the fracture network, i.e. $k_{fr} = k_{int} \cdot \tau$, where
219 k_{int} is the intrinsic permeability of the fracture network. The permeability of the fracture continuum, k_{fr}^c ,
220 is then conveniently expressed as:

$$(12)$$

221 The local matrix permeability, k_m , is subsequently set to several orders of magnitude less than k_{fr}^c and
222 may be determined via model calibration against laboratory data (Bandurraga and Bodvarsson 1999).
223 The permeability of the matrix continuum, k_m^c , is given by:

$$(13)$$

224 Equations (9) to (13) together define the approach used to assign the porosity and permeability under
225 the dual continuum framework considered in this work.

226 ***Mass exchange between the fracture and matrix continua***

227 Expressions for the sink/source terms controlling the exchange rates of inter-porosity water and
228 chemical components in the liquid and gas phases are presented in this section. It is assumed that quasi-
229 steady state distributions of pore water pressure and chemical concentrations prevail across the porous
230 matrix block thickness at all times. This assumption is strictly only valid once the pressure or
231 concentration front due to a change in conditions in the fracture network has reached the centre of the
232 matrix block, and so may not be valid over all time scales (Lemonnier and Bourbiaux 2010). However,
233 it allows the mass exchange terms to be conveniently expressed as linear functions of the differences
234 between the fracture and average matrix pressures and concentrations (Barenblatt, Zheltov et al. 1960,
235 Warren and Root 1963, Hassanzadeh, Pooladi-Darvish et al. 2009).

236 The mass exchange of water is treated as an advective flow, whereas for chemicals both advective and
237 diffusive mechanisms are considered (Gwo, Jardine et al. 1995, Ray, Ellsworth et al. 1997, Kohne,
238 Mohanty et al. 2004). Accordingly, first-order mass exchange terms can be written for water and the
239 dissolved chemical or gas component, expressed in a general form as (Gwo, Jardine et al. 1995, Ray,
240 Ellsworth et al. 1997):

$$\text{---} \quad (14)$$

$$\text{---} \quad (15)$$

241 where C_m is the resident concentration, for which $C_m = C_f$ if mass exchange is from the fracture
 242 continuum to the matrix continuum and $C_m = C_f$ if the exchange is reversed. λ_{ad} and λ_{di} are the first-
 243 order exchange rates relating to advection and diffusion, respectively. These parameters can be expanded
 244 considering the relevant geometrical and material properties, including the matrix block shape and
 245 dimensions, the permeability and diffusivity of the fracture-matrix interface (i.e. the fracture zone in
 246 Figure 2) and the fluid transport properties, giving expressions of the form (Schwartz, Juo et al. 2000):

$$\text{---} \quad (16)$$

$$\text{---} \quad (17)$$

247 where b is the typical half-width of a matrix block, K_{fm} is the effective hydraulic conductivity between
 248 the fracture and matrix pore regions, and α is a dimensionless factor related to the geometry of the
 249 matrix blocks, which can range from 3 for rectangular slabs to 15 for spherical aggregates (Gerke and
 250 van Genuchten 1993, Kohne, Mohanty et al. 2004), but otherwise in practice may also be lumped with
 251 the remaining parameters in equations (16) and (17) to form an empirical coefficient for calibration
 252 using observed laboratory or field data. Gerke and van Genuchten (1993) evaluated a number of methods
 253 for obtaining α and concluded that an arithmetic mean approach is the most practical, giving:

$$\text{---} \quad (18)$$

254 ***Chemical reactions***

255 Previous works have coupled the transport model (COMPASS) with chemical models, for example
 256 MINTEQA2 (Cleall, Seetharam et al. 2007, Seetharam, Thomas et al. 2007) and PHREEQC (version 2)
 257 (Thomas, Sedighi et al. 2012, Sedighi, Thomas et al. 2015), enabling the study of a range of
 258 geoenvironmental and geoenergy problems involving multiphase, multicomponent chemical transport
 259 in single porosity geomaterials with homogenous and heterogeneous reactions. While an extension of

260 this coupling to the dual porosity framework is not part of the present developments, which are more
 261 concerned with transport processes than chemical reactions, it is considered for future development as
 262 has already been accomplished in other applications of COMPASS (e.g. Sedighi, Thomas et al. 2016).
 263 Nonetheless, the adsorption and desorption of multicomponent chemicals is important in geoenery
 264 applications including carbon sequestration in coal, enhanced hydrocarbon recovery, and
 265 unconventional gas exploration. Hence, the development of the chemical reactions presented is limited
 266 here to adsorption and desorption in the solid, and it is acknowledged that a more general geochemical
 267 modelling approach will be required when a further complicated multiphase, multicomponent system is
 268 of interest.

269 The sink/source terms, S , in equations (1) and (2) can be expanded to give:

$$\frac{\partial S}{\partial t} = \rho_b \frac{\partial q}{\partial t} \quad (19)$$

$$S = \rho_b (q - q_0) \quad (20)$$

270 where ρ_b is the dry bulk density, q is the adsorbed amount of the chemical component. The factors
 271 ρ_b and ρ_b are used to partition the adsorption sites between the fracture network and porous
 272 matrix blocks.

273 Adsorption inherently depends on the available surface area of the adsorbent (solid phase) over which
 274 interactions with the adsorbate can occur. In fractured rock, such as coal, the majority of the surface area
 275 exists in the porous matrix blocks (Clarkson and Bustin 2010). It is therefore assumed that the matrix
 276 continuum provides all of the adsorption capacity, so that equations (19) and (20) become:

$$\frac{\partial S}{\partial t} = \rho_b \frac{\partial q}{\partial t} \quad (21)$$

$$S = \rho_b (q - q_0) \quad (22)$$

277 A kinetic chemical reaction is formulated to describe the adsorption/desorption phenomena, similar to
 278 that presented in the previous section for inter-porosity mass exchange. This yields a first-order model
 279 describing sorption in the matrix continuum, as (King, Ertekin et al. 1986):

$$\frac{dQ}{dt} = -k_d \left(\frac{Q}{Q_{eq}} - 1 \right) \quad (23)$$

280 where Q is the rate of adsorption/desorption and Q_{eq} is the adsorbed amount at equilibrium with the
 281 free-phase adsorbate. k_d is evaluated using an appropriate adsorption isotherm, which may be a
 282 simple linear relationship or a nonlinear relationship such as a Langmuir isotherm.

283 *Multiphase coupling*

284 Changes in the degree of water saturation, S_w , influence the physical and chemical behaviour in
 285 partially saturated fractured rock, most notably through feedback to the phase relative permeability,
 286 $k_{r,w}$. An important characteristic of fractured rock is that the fracture network is more free-draining
 287 than the porous rock matrix, making it important to define the water retention behaviour appropriately
 288 in the respective continua. The rate of change of S_w is affected by the difference between pore water
 289 pressure and pore gas pressure, known as matric suction (Mitchell and Soga 2005), as well as changes
 290 to the void ratio caused by deformation (Gallipoli, Wheeler et al. 2003). The effect of the latter is less
 291 clearly defined and often neglected in the study of fairly rigid porous media (Mašín 2010), such as coal,
 292 giving:

$$\frac{dS_w}{dt} = -\frac{1}{\alpha} \frac{dS_u}{dt} \quad (24)$$

293 where S_u is the matric suction, expressed in terms of the primary variables with substitution from
 294 equation (7), leading to (Mitchell and Soga 2005):

$$S_u = p_g - p_w \quad (25)$$

295 From equations (24) and (25), the temporal derivative of the degree of water saturation can be expanded
 296 to yield:

$$\frac{dS_w}{dt} = -\frac{1}{\alpha} \left(\frac{\partial S_w}{\partial p_g} \frac{dp_g}{dt} - \frac{\partial S_w}{\partial p_w} \frac{dp_w}{dt} \right) \quad (26)$$

297 where the partial derivative of S_w with respect to p_g is analogous to the specific water capacity and
 298 defined as the gradient of the water retention curve via the van Genuchten (1980) model, given by:

(27)

299 where θ_w is the effective volumetric water content, and $\theta_{r,w}$ and $\theta_{s,w}$ are the residual and saturated
300 volumetric water contents, respectively, and α_n , β_n and γ_n ($n = 1, 2$) are constants based on the
301 water retention characteristics of each continuum.

302 The phase relative permeability, $k_{r,w}^n$, is evaluated from θ_w , giving:

(28)

303 where the function on the right hand side is given by the van Genuchten-Mualem model (Mualem 1976,
304 van Genuchten 1980) for $n = 1$, with the extended model by Parker et al. (1987) used for $n = 2$, giving:

(29)

(30)

305 The main limitation of this approach in the dual porosity framework is the lack of experimental data
306 available to determine the parameters of the hydraulic functions given in equations (27), (29) and (30).
307 Nonetheless, it is possible to estimate water retention curves for the fracture and matrix continua based
308 on the characteristics of the respective pore regions, most notably the pore size distributions (e.g. Zhang
309 and Fredlund 2003). Moreover, Köhne et al. (2002) presented a procedure for estimating the dual
310 permeability water retention and conductivity functions using bulk soil data, based on the notion of
311 volumetric weighting. Since volumetric weighting is also used in this formulation, future work could
312 look at applying the Köhne et al. procedure for modelling fractured rock.

313 Further to the water retention behaviour and phase relative permeability described in this section, the
314 option to include gas-liquid phase transformations exists through the coupling of COMPASS with
315 PHREEQC. However, this option has not been explored in the present work owing to the focus on
316 carbon sequestration in coalbeds, in which the adsorbed phase tends to dominate gas storage. Coalbeds
317 are also quite often dewatered during primary methane recovery prior to the injection of carbon dioxide
318 (CO_2) for enhanced recovery. Further applications of the model considering problems such as carbon
319 sequestration in saline aquifers would require an elaboration of the gas-liquid phase transformation.

320 **Gas properties**

321 Appropriate constitutive relationships are employed in the model to accurately describe the evolution of
322 the key gas transport properties as the pressure, temperature and composition vary. In relation to the
323 formulation described above, these properties are the non-ideal gas compressibility and the gas viscosity.
324 Non-ideal gas compressibility is considered using the Peng and Robinson (1976) equation of state (EoS)
325 with van der Waals mixing rules. This approach has been widely applied with a proven accuracy and
326 requires little input data (Wei and Sadus 2000). The EoS expresses the bulk gas pressure as:

$$\frac{P}{RT} = \frac{1}{V - b} - \frac{a}{V(V + b)} \quad (31)$$

327 where b is the effective volume of the molecules contained in one mole of bulk gas and a is a
328 coefficient accounting for the intermolecular interactions in the mixture, both of which are obtained via
329 the van der Waals mixing rules (Kwak and Mansoori 1986). The parameter V is the molar volume of
330 the gas mixture predicted by the ideal gas law.

331 For an ideal gas, the factors a and b are zero and equation (31) reduces to the ideal gas law. However,
332 the ideal gas law does not accurately describe the pressure-volume-temperature characteristics of gas
333 under the majority of conditions (Dake 1978). Deviations from the ideal gas law are described by the
334 compressibility factor, Z , which is determined by rewriting equation (31) as a cubic equation according
335 to Peng and Robinson (1976):

$$Z^3 - Z^2 + \frac{a}{RT} Z - \frac{b}{RT} = 0 \quad (32)$$

336 where:

$$a = \sum_i \sum_j y_i y_j a_{ij} \quad (33)$$

$$b = \sum_i y_i b_i \quad (34)$$

337 Of the three roots to Equation (32), the selection of Z depends on the number of real roots and the phase
338 composition of the pore fluid, as outlined by Chen et al. (2006).

339 Gas mixture viscosity is included using the semi-empirical model proposed by Chung et al. (1988). The

340 model is based on the kinetic theory of gases in combination with empirical density-dependent functions
 341 and has been chosen ahead of simpler interpolative models because it describes the evolution of the
 342 mixture viscosity not only with composition, but also with pressure and temperature. Moreover, the
 343 model retains accuracy near the critical point and has shown absolute deviations of no more than 9% for
 344 non-polar dense gas mixtures. The model is expressed as:

$$(35)$$

345 where μ_0 is a function of the gas mixture viscosity at low pressure and α is an adjustment for
 346 dense gases. These terms are fully expanded and described in Chung et al. (1988).

347 ***Deformation feedback***

348 While mechanical behaviour is not explicitly considered in this work, the feedback of deformation on
 349 fluid transport is considered implicitly since it can be important in some cases of dual porosity flow. For
 350 example, the porosity and permeability of rock can be strongly influenced by effective stress changes
 351 and certain chemo-mechanical phenomena, including sorption-induced swelling/shrinking of the rock
 352 matrix. These changes in porosity and permeability are described in a general form as (Xu and Pruess
 353 2001):

$$\frac{\mu}{\mu_0} = \frac{1}{1 + \alpha \left(\frac{\sigma - \sigma_0}{\sigma_0} + \epsilon \right)} \quad (36)$$

354 where the subscript 0 denotes the initial condition, σ is the effective stress, and ϵ is the total sorption
 355 strain of the matrix blocks, equal to the sum of the strains induced by each component, i.e. $\epsilon = \sum \epsilon_i$.

356 Relationships in the form of equation (36) apply in the study of geomaterials which can be described as
 357 fractured sorptive elastic media (e.g. coal). A number of relationships have been presented in the
 358 literature (Palmer and Mansoori 1988, Shi and Durucan 2004, Robertson and Christiansen 2008), with
 359 an adsorption isotherm-type relationship conventionally being used to obtain ϵ . This approach has
 360 proven accurate based on comparison with the results of experimental studies (Harpalani and Chen 1995,
 361 Levine 1996).

362 **Computational approach**

363 Substitution of the pore fluid velocity from equation (5), the porosity and permeability relationships
364 from equations (9) to (13), the mass exchange sink/source terms from equations (14) and (15), and the
365 chemical reaction sink/source term from equations (22) and (23) into equations (1) and (2) produces
366 equations of the form:

$$\frac{\partial}{\partial t} \left(\frac{\rho_w}{\rho_w} \right) + \frac{\partial}{\partial x} \left(\frac{\rho_w}{\rho_w} \right) = \frac{\rho_w}{\rho_w} \quad (37)$$

$$\frac{\partial}{\partial t} \left(\frac{\rho_w}{\rho_w} \right) + \frac{\partial}{\partial x} \left(\frac{\rho_w}{\rho_w} \right) + \frac{\partial}{\partial x} \left(\frac{\rho_w}{\rho_w} \right) = \frac{\rho_w}{\rho_w} \quad (38)$$

367 where α and β are lumped coefficients of the governing equations, and γ and δ are terms
368 representing the gravitational body forces for the water and chemical terms, respectively.

369 The numerical solution of the governing equations is achieved by applying the finite element method
370 with Galerkin weighted residuals for spatial discretisation and an implicit mid-interval backward-
371 difference scheme for temporal discretisation. This solution procedure follows works on the coupled
372 THM and THCM behaviour of single porosity media presented in detail by Thomas and He (1998) and
373 Seetharam et al. (2007). A time splitting technique, namely the sequential non-iterative approach
374 (SNIA), is employed in which the conservative transport formulation, mass exchange and chemical
375 reactions are solved sequentially in each time step. In other words, each time step first involves solving
376 the conservative transport equations in each continuum assuming no mass exchange and no reactions.
377 Once this system has converged, the values of the primary flow variables are updated in the mass
378 exchange and chemical reaction modules. Although such an approach has proven successful for
379 sufficiently small time steps (Seetharam, Thomas et al. 2007, Thomas, Sedighi et al. 2012), the use of a
380 split time step via the SNIA is acknowledged as a limitation of the present work and other approaches,
381 including the sequential iterative approach (SIA) and global implicit approach, are available.

382 **Model verification**

383 A set of verification tests has been performed to assess the correctness of the numerical implementation

384 of the theoretical and numerical developments in the model, with benchmarks provided by analytical or
385 alternative numerical solutions presented in the literature. The first test deals with multiphase flow,
386 considering the evolution of the degree of saturation as water and gas flow in a partially saturated porous
387 medium. In the second test, two simulations are performed for multicomponent gas transport at high
388 pressure with kinetically-controlled adsorption/desorption. The results are compared with the results of
389 an alternative numerical model presented in the literature. This also provides an opportunity to verify
390 the performance of the constitutive relationships implemented for non-ideal gas behaviour, most notably
391 in the case of CO₂ transport, which is highly non-ideal under the simulation conditions. A further sets
392 of tests is then presented to examine the coupling scheme (SNIA) between the chemical transport and
393 inter-porosity mass exchange modules of the developed model.

394 *Multiphase flow*

395 This section presents a verification test (Test I) for the coupled flow of water and ideal gas in a single
396 porosity medium. The test considers a two-dimensional domain of 1 m length and 0.1 m height, spatially
397 discretised using 200 quadrilateral elements concentrated towards the upstream and downstream faces.
398 Under the simulation conditions shown in Figure 3, the isothermal system is initially partially saturated
399 with fixed pore water and gas pressures at the downstream boundary. An influx of gas begins at the
400 upstream boundary after 1 day, rising linearly from zero to 0.01 mol s⁻¹ by the end of the s
401 simulation period. The aim of the test is to verify the initial ingress of water from the downstream
402 boundary and its subsequent displacement due to the gas influx at the upstream boundary.

403 A benchmark for the simulation results is provided by comparing the predicted changes in the degree of
404 water saturation to the conditions expected with reference to the water retention and relative
405 permeability functions in Figure 4 and Figure 5, respectively, based on the material parameters provided
406 in Table 1. Similar to the approach of Köhne et al. (2002), the parameters adopted for the hydraulic
407 functions are taken from van Genuchten (1980) and compare an un-fractured rock matrix to a fine-
408 textured porous medium, in this case “Touchet silt loam”.

409 Figure 6 shows the predicted evolution of the degree of water saturation, θ , at the mid-point of the
410 domain, i.e. $x = 0.5$ m. The first point of reference for θ is under the initial conditions, given as 0.81

411 by the flat section of Figure 6 at early times before water ingress from the downstream boundary.
412 Considering the initial suction of 18.1 kPa, the initial θ predicted in the numerical simulation agrees
413 with the expected value given by Figure 4. After this initial period, θ rises towards the fully saturated
414 condition as the flow of water from the downstream boundary reaches the mid-point of the domain, with
415 this condition prevailing until the onset of gas injection after 1 day (86400 s). As expected, the gas
416 influx from the upstream boundary causes a decline in θ , initially sharp before tailing as it tends towards
417 the residual value of 0.405. Noting the logarithmic scales used for the time axes, the tailing of θ in
418 Figure 6 as the gas flux increases is comparable to that of the water retention curve in Figure 4. In other
419 words, θ is declining in the manner expected as the pore gas pressure in the system steadily increases.

420 Test I demonstrates the capability for simulating two-phase flow under the conditions considered,
421 namely, the re-saturation of a partially saturated porous medium and the subsequent displacement of
422 pore water through gas injection. The test therefore forms the basis for further verification of multiphase
423 flow in future work, particularly for the dual porosity case, where inter-porosity flow and the bi-modal
424 nature of the hydraulic functions are of relevance.

425 ***Multicomponent reactive gas transport at high pressure***

426 Two scenarios of high pressure gas injection and displacement are simulated and the results are
427 compared with those obtained in the numerical modelling study by Pini et al. (2011). Both scenarios
428 deal with the enhanced displacement of methane (CH₄) due to gas injection in a 100 m long coalbed
429 with unit cross section. The first scenario (Test II-a) considers the displacement of CH₄ during CO₂
430 injection, i.e. carbon sequestration, whereas the second scenario (Test II-b) considers nitrogen (N₂)
431 injection.

432 Since the exercise is mainly concerned with verifying the non-ideal, multicomponent reactive gas
433 transport behaviour, the system is treated as a single porosity medium with kinetically-controlled
434 adsorption/desorption. The domain is discretised using 500 equally-sized 4-noded quadrilateral elements
435 and is initially saturated with CH₄ at a pressure of 1.5 MPa at a temperature of 318 K. The amount of
436 gas stored in the adsorbed phase is initially at equilibrium with the free gas phase and calculated using

437 the extended Langmuir isotherm (ELI), which for the component in a gas mixture is given by
 438 (Ruthven 1984):

$$(39)$$

439 where is the Langmuir capacity and is the reciprocal of the Langmuir pressure. Equation (39) is
 440 used in equation (23) to calculate the changes in the adsorbed phase as CO₂ or N₂ displaces CH₄ in the
 441 coalbed.

442 The injection boundary pressure for CO₂ and N₂ is 4 MPa at , with an atmospheric pressure
 443 production boundary condition prescribed at . A schematic representation of this system is

Injection boundary conditions	Initial conditions	Production boundary conditions
Test II-a: $c_g^{CO_2} = 1,881.9 \text{ mol m}^{-3}$	Free gas (mol m ⁻³): $c_g^{CO_2} = c_g^{N_2} = 0.0$ $c_g^{CH_4} = 582.4$	$RT \sum_{j=1}^{n_g} c_g^j$ $= 0.1 \times 10^6 \text{ Pa}$ $\sum_{j=1}^{n_g} \frac{\partial c_g^j}{\partial t} = 0.0$
Test II-b: $c_g^{N_2} = 1,522.5 \text{ mol m}^{-3}$	Adsorbed gas (mol kg ⁻¹): $s_{gM}^{CO_2} = s_{gM}^{N_2} = 0.0$ $s_{gM}^{CH_4} = 0.75$	

444 provided in

445 Figure 7, where the stated pressures are expressed as the equivalent gas concentrations. All of the gas
 446 properties required in the Peng and Robinson EoS have been taken from IEAGHG (2011).

447 As adopted by Pini et al. (2011), in equation (36) is expanded using the relationship proposed
 448 by Gilman and Beckie (2000), giving:

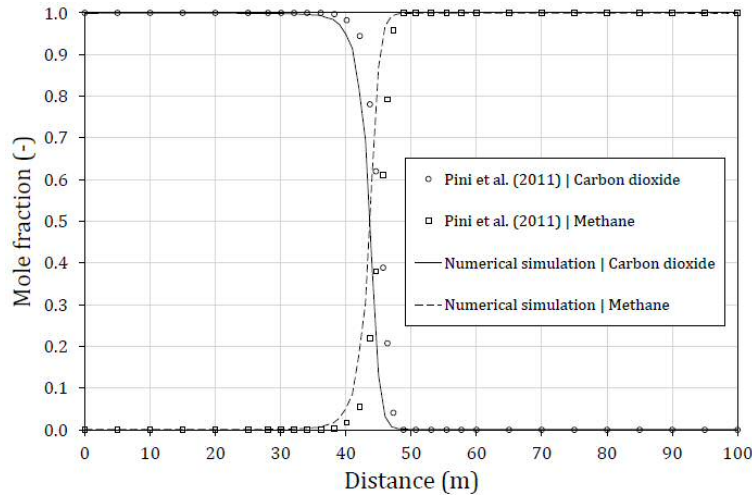
$$(40)$$

449 where is Poisson's ratio, is Young's modulus, is the confining pressure, and the coefficients
 450 and are defined in Table 2.

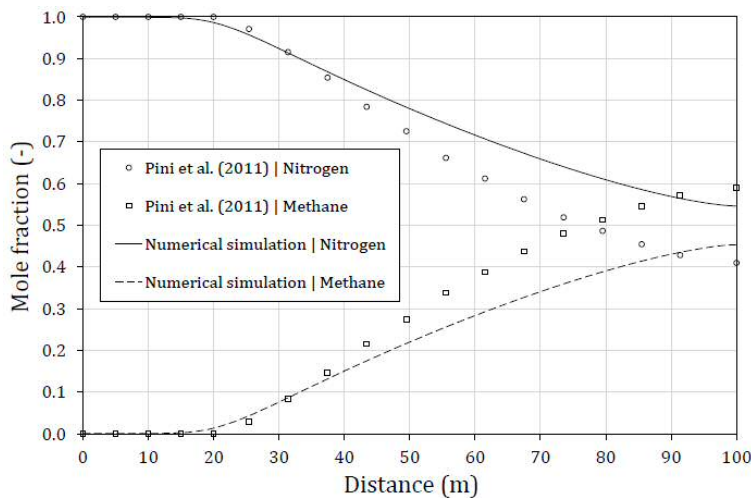
451 along with a summary of the other physical and chemical parameters used in the simulations, including
 452 the component viscosities, , adopted from Linstrom and Mallard (2001). The parameter is the
 453 swelling fraction, i.e. , with given by:

454 where ϵ_L is the Langmuir strain and λ is the reciprocal of the Langmuir swelling pressure.

455



456



457 Figure 8 and

458 Figure 9 show the results obtained using the numerical model after 42 days of analysis for Tests II-a and

459 II-b, respectively. There are considerable differences in the predicted CH_4 displacement profiles, with

460 CO_2 producing a sharper yet less advanced front compared to the results for N_2 injection. Whilst both

461 gases physically sweep free CH_4 from the pore space, these differences arise due to the sorption and

462 sorption-induced swelling phenomena. In particular: i) coal has a higher affinity for CO_2 adsorption than

463 for CH_4 , whereas a lower affinity for N_2 adsorption, and ii) CO_2 adsorption results in a swelling-induced

464 permeability loss. Hence, in Test II-b, N_2 does not displace the adsorbed CH_4 as efficiently as CO_2 in

465 Test II-a, less N₂ is immobilised via adsorption, and the system permeability remains higher. The
466 displacement of the free CH₄ therefore occurs more rapidly in Test II-b, causing breakthrough of N₂ at
467 the production boundary. The significant spreading of the injection front can be attributed to the more
468 gradual displacement of the adsorbed CH₄ by N₂ compared to CO₂.

469 In both tests, the results show agreement with the benchmarks provided by Pini et al. (2011). A degree
470 of deviation is noted and may be attributed to differences in the prescribed gas viscosities. Whereas Pini
471 et al. adopted Wilke's dilute gas mixture method (Poling, Prausnitz et al. 2001) using unspecified pure
472 component viscosities, the same method has been used here for Test II but with viscosities taken from
473 Linstrom and Mallard (2001). Hence, there may be some degree of disagreement between these
474 viscosities and those used by Pini et al. Based on the results achieved and under the conditions of the
475 problems described, it can be reasonably concluded that the transport behaviour of multicomponent gas,
476 including kinetically-controlled adsorption/desorption, is accurately implemented in the numerical
477 model.

478 *Dual porosity, dual permeability chemical transport and exchange*

479 This section presents three verification tests (Tests III-a, III-b and III-c) for dual porosity, dual
480 permeability chemical transport. The tests consider the transport of a chemical component in a fully
481 saturated dual porosity geomaterial subject to steady state water flow, equilibrium adsorption, and
482 various mass exchange rates. The simulation results are presented as chemical breakthrough curves at
483 an analysis point and comparisons are made with the results obtained by Šimunek and van Genuchten
484 (2008) using the HYDRUS-1D numerical model.

485 A two-dimensional domain of 1 m length and 0.1 m height is spatially discretised using 50 equally-sized
486 4-noded quadrilateral elements, with the analysis point for chemical breakthrough located at $x = 0.5$ m.
487 Each test is performed for a simulation period of 10 days with initial and maximum time steps of 100
488 and 3,600 seconds, respectively. The arbitrary chemical component is introduced into the system with a
489 fixed concentration of 1 mol m^{-3} at $x = 0$ m and a far field concentration of 0 mol m^{-3} at $x = 1$ m.

490 Diffusion of the chemical was not considered by Šimunek and van Genuchten (2008) and equilibrium

491 adsorption was modelled using a retardation factor, R . Under these conditions, the governing equation
 492 in equation (2) reduces to:

$$\frac{\partial C}{\partial t} + \frac{\partial C}{\partial x} = \frac{D}{R} \frac{\partial^2 C}{\partial x^2} \quad (42)$$

493 with the coefficient of mechanical dispersion, D , given by:

$$D = D_m + \alpha_L v \quad (43)$$

494 where α_L is the longitudinal dispersivity.

495 Since the pore water pressures in the fracture and matrix continua are assumed to remain equilibrated,
 496 the advective component of chemical mass exchange in equation (15) becomes zero. Šimunek and van
 497 Genuchten (2008) then used a lumped mass exchange rate for the diffusive component, given by:

$$\lambda = \lambda_m \quad (44)$$

498 with the mass exchange rate, λ , defined as:

$$\lambda = \frac{dC_m}{dt} \quad (45)$$

$$\lambda = \frac{dC_f}{dt} \quad (46)$$

499 where λ is the chemical mass exchange rate.

500 HYDRUS-1D handles the dual porosity, dual permeability framework in a slightly different form to that
 501 described in this work. Based on the work of Gerke and van Genuchten (1993), the material parameters
 502 in the governing equations are defined at the local scale (e.g. α_L), whereas in this work they are
 503 defined at the bulk scale (e.g. α_L). A discussion on the background and procedures for converting
 504 between the local and bulk scales was provided in the “Porosity and permeability” section of the
 505 theoretical formulation. Importantly, both approaches produce the same overall behaviour.

506 As an example, Šimunek and van Genuchten (2008) set λ as 0.1 and prescribed steady pore water
 507 velocities of 1 m s^{-1} and 0.1 m s^{-1} at the local scale in the fracture and matrix
 508 continua, respectively. The corresponding bulk scale hydraulic conductivities are back-calculated from

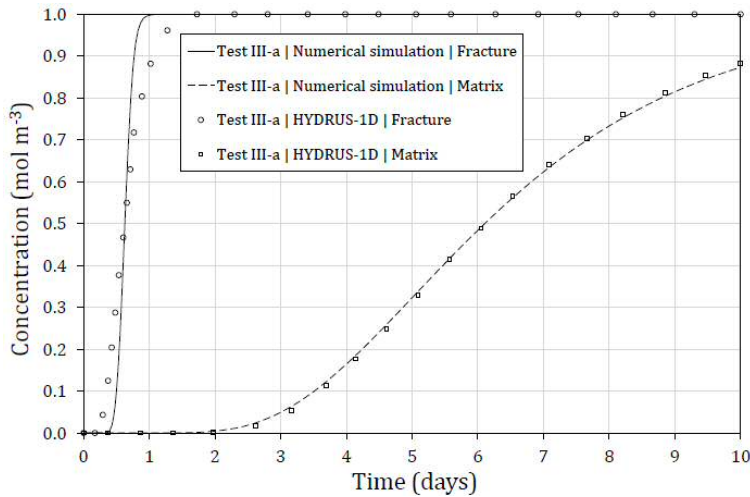
509 these velocities using equation (5) () by prescribing a pressure drop of 10 Pa over the length
 510 of the domain and using to convert to the equivalent bulk scale conductivities, giving:

$$\text{-----} \tag{47}$$

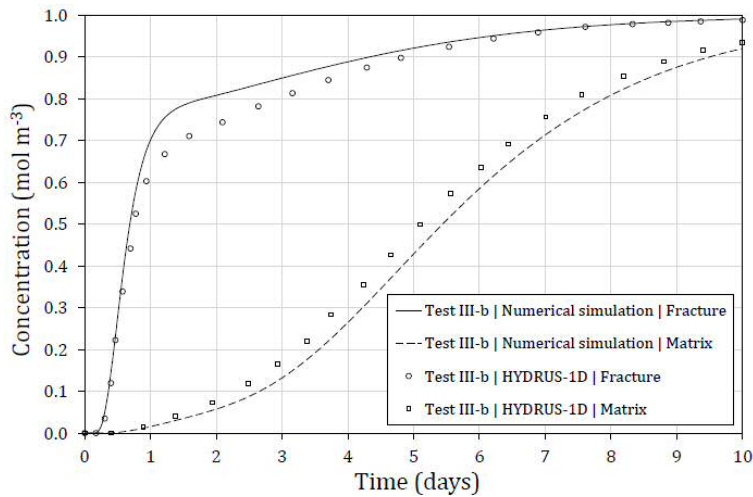
$$\text{-----} \tag{48}$$

511 where is the pore water velocity at the local pore region scale, is the length of the domain, i.e. 1 m,
 512 and Pa, giving m s^{-1} and m s^{-1} .

513 Table 3 provides a summary of the physical and chemical parameters used in the simulations for
 514 verification Tests III-a, III-b and III-c. No mass exchange is considered in Test III-a so that the fracture
 515 and matrix continua behave as independent flow conduits. The effects of different mass exchange rates
 516 are then examined in Tests III-b and III-c, with the rate in Test III-c being five times greater than that
 517 applied in Test III-b.



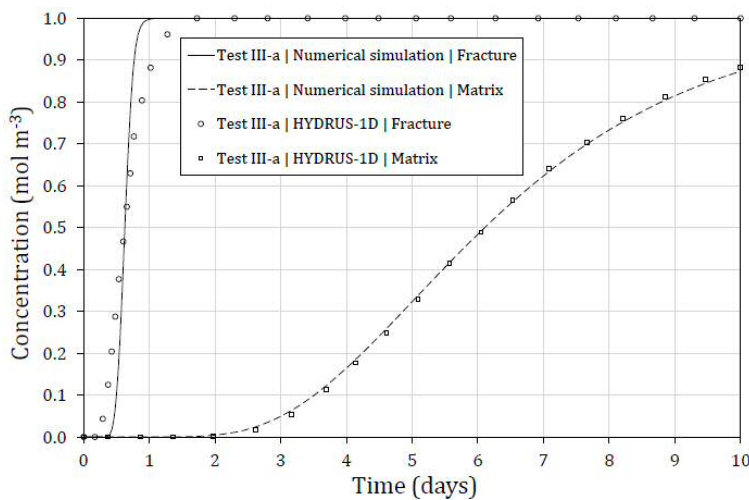
518
 519 Figure 10 shows the chemical breakthrough in the fracture and matrix continua with no mass exchange.
 520 It can be seen that the breakthrough in the fracture continuum occurs earlier and is sharper than in the
 521 matrix continuum. This results from a combination of the higher pore water velocity in the fracture
 522 continuum and the considerably lower chemical storage capacity provided by its porosity.



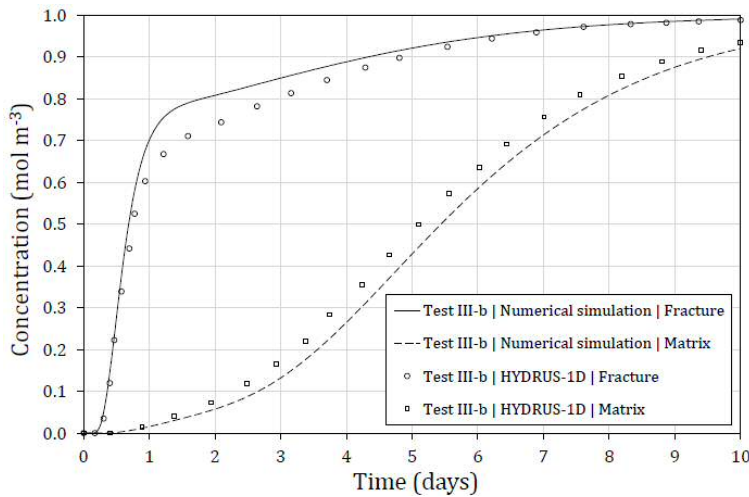
523 The breakthrough curves in

524 Figure 11 and Figure 12 show the role of lower (Test III-b) and higher (Test III-c) mass exchange rates
 525 on chemical transport, respectively. Most notable are the more gradual fracture breakthrough and earlier
 526 matrix breakthrough which follow an increase in the mass exchange rate. This is the expected trend
 527 since the rapid chemical advance in the fracture continuum resulted in higher fracture concentrations
 528 than matrix concentrations, thereby driving chemical exchange from the fracture continuum into the
 529 matrix continuum. At higher mass exchange rates the resistance to these flow interactions between the
 530 continua reduces. The breakthrough curves then tend towards that which would be predicted by an
 531 equivalent single porosity, single permeability model.

532 Having analysed the breakthrough curves in



533



534 Figure 10,

535 Figure 11 and Figure 12, it can be concluded that the sink/source term for mass exchange between the
 536 fracture and matrix continua produces the expected behaviour. Further confidence is provided by the
 537 close agreement of the results with the benchmarks provided by Šimunek and van Genuchten (2008) for
 538 HYDRUS-1D.

539 The set of verification tests presented above establish a good level of confidence regarding the accurate
 540 numerical implementation of the theoretical framework for reactive flow in dual porosity geomaterials.
 541 Building upon this work, the application of the model in the study of geoenery applications, such as
 542 geological carbon sequestration, will be considered in future work.

543 **Conclusions**

544 A theoretical and numerical modelling platform has been developed for studying the coupled behaviour
 545 of geoenery systems involving the transport, storage, and displacement of multiphase, multicomponent
 546 chemicals and gas in the deep geoenvironment. Specifically, the capabilities of a coupled thermal,
 547 hydraulic, chemical and mechanical (THCM) model have been enhanced to consider hydraulic,
 548 chemical, gas and deformation behaviour based on a dual porosity, dual permeability framework.

549 Appropriate constitutive relationships have been included to provide an accurate description of the
 550 properties of high pressure, non-ideal gas mixtures. Additional theoretical features have also been
 551 included to allow the study of physically and chemically complex geomaterials, such as coal. There are
 552 terms in the governing equations to describe equilibrium or kinetically-controlled adsorption/desorption

553 in the porous matrix, and an implicit approach has been employed to consider the feedback of physico-
554 and chemo-mechanical deformation on the transport processes.

555 A set of verification tests of the model provided further confidence in: i) the approach taken to
556 multiphase coupling, ii) the accuracy of the numerical implementation of the dual porosity governing
557 equations, and iii) the effectiveness of the technique employed for coupling the transport module with
558 the mass exchange and chemical reaction modules. The tests have been accompanied by analyses of the
559 relevant behaviour considered, lending further confidence to the verification process.

560 The compositional structure of the model developed provides a flexible scientific tool for both present
561 and future applications in the geoenergy field. The developments are most relevant to the simulation of
562 high pressure gas transport, storage, and displacement in fractured rock during geological carbon
563 sequestration, the enhanced recovery of conventional oil and gas, the exploration of unconventional gas,
564 and the deep geological disposal of nuclear waste. Nonetheless, the model can be more generally applied
565 in the study of other geoenvironmental problems in structured soils, including groundwater flow and
566 contaminant transport. Hence, future work will focus on the application of the model to enhance the
567 current understanding in these geoenergy and geoenvironmental areas.

568 **Acknowledgements**

569 The financial support provided by the Welsh European Funding Office (WEFO) for the PhD studentship
570 of the first author, through the Seren project, is gratefully acknowledged.

References

- Bai, M., Elsworth, D. and Roegiers, J. C. 1993. Multiporosity Multipermeability Approach to the Simulation of Naturally Fractured Reservoirs. *Water Resources Research*, **29**(6): 1621-1633.
- Bandurraga, T. M. and Bodvarsson, G. S. 1999. Calibrating hydrogeologic parameters for the 3-D site-scale unsaturated zone model of Yucca Mountain, Nevada. *Journal of Contaminant Hydrology*, **38**(1-3): 25-46.
- Barenblatt, G. I., Zheltov, I. P. and Kochina, I. N. 1960. Basic concepts in the theory of seepage of homogenous liquids in fissured rocks (strata). *Journal of Applied Mathematics and Mechanics*, **24**(5): 1286-1303.
- Bear, J., Ed. 1993. Modeling flow and contaminant transport in fractured rocks. Flow and contaminant transport in fractured rock, Academic Press, Inc.
- Bear, J. and Verruijt, A. 1987. Modeling groundwater flow and pollution. Dordrecht, The Netherlands, D. Reidel Publishing Company.
- Berkowitz, B. 2002. Characterizing flow and transport in fractured geological media: A review. *Advances in Water Resources*, **25**(8-12): 861-884.
- Chen, Z., Huan, G. and Ma, Y. 2006. Computational Methods for Multiphase Flows in Porous Media. Philadelphia, Society for Industrial and Applied Mathematics.
- Chung, T. H., Ajlan, M., Lee, L. L. and Starling, K. E. 1988. Generalized Multiparameter Correlation for Nonpolar and Polar Fluid Transport-Properties. *Industrial & Engineering Chemistry Research*, **27**(4): 671-679.
- Clarkson, C. R. and Bustin, R. M. 1999. The effect of pore structure and gas pressure upon the transport properties of coal: a laboratory and modeling study. 2. Adsorption rate modeling. *Fuel*, **78**(11): 1345-1362.
- Clarkson, C. R. and Bustin, R. M. 2010. Coalbed methane: current evaluation methods, future technical challenges. SPE Unconventional Gas Conference. Pittsburgh, Pennsylvania.
- Cleall, P. J., Seetharam, S. C. and Thomas, H. R. 2007. Inclusion of some aspects of chemical behavior of unsaturated soil in thermo/hydro/chemical/mechanical models. I: Model development. *Journal of Engineering Mechanics-Asce*, **133**(3): 338-347.
- Cussler, E. L. 1997. Diffusion: mass transfer in fluid systems. Cambridge, Cambridge University Press.

- Dake, L. P. 1978. Fundamentals of reservoir engineering. Amsterdam, The Netherlands, Elsevier.
- Di Donato, G. and Blunt, M. J. 2004. Streamline-based dual-porosity simulation of reactive transport and flow in fractured reservoirs. *Water Resources Research*, **40**(4).
- Gallipoli, D., Wheeler, S. and Karstunen, M. 2003. Modelling the variation of degree of saturation in a deformable unsaturated soil. *Géotechnique*, **53**(1): 105-112.
- Gerke, H. H. and van Genuchten, M. T. 1993. A Dual-Porosity Model for Simulating the Preferential Movement of Water and Solutes in Structured Porous-Media. *Water Resources Research*, **29**(2): 305-319.
- Gerke, H. H. and van Genuchten, M. T. 1993. Evaluation of a First-Order Water Transfer Term for Variably Saturated Dual-Porosity Flow Models. *Water Resources Research*, **29**(4): 1225-1238.
- Gilman, A. and Beckie, R. 2000. Flow of coal-bed methane to a gallery. *Transport in Porous Media*, **41**(1): 1-16.
- Gwo, J. P., Jardine, P. M., Wilson, G. V. and Yeh, G. T. 1995. A Multiple-Pore-Region Concept to Modeling Mass-Transfer in Subsurface Media. *Journal of Hydrology*, **164**(1-4): 217-237.
- Harpalani, S. and Chen, G. L. 1995. Estimation of Changes in Fracture Porosity of Coal with Gas Emission. *Fuel*, **74**(10): 1491-1498.
- Hassanzadeh, H., Pooladi-Darvish, M. and Atabay, S. 2009. Shape factor in the drawdown solution for well testing of dual-porosity systems. *Advances in Water Resources*, **32**(11): 1652-1663.
- Hosking, L. J. 2014. Reactive transport modelling of high pressure gas flow in coal, Cardiff University.
- IEAGHG 2011. Effects of impurities on geological storage of CO₂, International Energy Agency Environmental Projects Ltd.
- King, G. R., Ertekin, T. and Schwerer, F. C. 1986. Numerical simulation of the transient behaviour of coal-seam degasification wells. *Society of Petroleum Engineers Formation Evaluation*, **1**(2): 165-183.
- Köhne, J. M., Köhne, S. and Gerke, H. 2002. Estimating the hydraulic functions of dual-permeability models from bulk soil data. *Water resources research*, **38**(7).
- Kohne, J. M., Mohanty, B. P., Simunek, J. and Gerke, H. H. 2004. Numerical evaluation of a second-order water transfer term for variably saturated dual-permeability models. *Water Resources Research*, **40**(7).

- Kwak, T. Y. and Mansoori, G. A. 1986. Vanderwaals Mixing Rules for Cubic Equations of State - Applications for Supercritical Fluid Extraction Modeling. *Chemical Engineering Science*, **41**(5): 1303-1309.
- Lemonnier, P. and Bourbiaux, B. 2010. Simulation of Naturally Fractured Reservoirs. State of the Art-Part 2-Matrix-Fracture Transfers and Typical Features of Numerical Studies. *Oil & Gas Science and Technology- Revue de l'Institut Français du Pétrole*, **65**(2): 263-286.
- Levine, J. R. 1996. Model study of the influence of matrix shrinkage on absolute permeability of coal bed reservoirs. In Gayer, R. & Harris, I. (eds.) *Coalbed methane and coal geology*: 197-212.
- Linstrom, P. J. and Mallard, W. G. 2001. NIST Chemistry WebBook; NIST Standard Reference Database No. 69. from <http://webbook.nist.gov/>.
- MacQuarrie, K. T. B. and Mayer, K. U. 2005. Reactive transport modeling in fractured rock: A state-of-the-science review. *Earth-Science Reviews*, **72**(3-4): 189-227.
- Mašín, D. 2010. Predicting the dependency of a degree of saturation on void ratio and suction using effective stress principle for unsaturated soils. *International Journal for Numerical and Analytical Methods in Geomechanics*, **34**(1): 73-90.
- Masum, S. A. 2012. Modelling of reactive gas transport in unsaturated soil – a coupled thermo-hydro-chemical-mechanical approach PhD Thesis, Cardiff University.
- Mitchell, J. K. and Soga, K. 2005. *Fundamentals of soil behavior*.
- Mualem, Y. 1976. A new model for predicting the hydraulic conductivity of unsaturated porous media. *Water resources research*, **12**(3): 513-522.
- Ozdemir, E. 2009. Modeling of coal bed methane (CBM) production and CO₂ sequestration in coal seams. *International Journal of Coal Geology*, **77**(1-2): 145-152.
- Palmer, I. and Mansoori, J. 1988. How permeability depends on stress and pore pressure in coalbeds: a new model. *Spe Reservoir Evaluation & Engineering*, **1**(6): 539-544.
- Parker, J., Lenhard, R. and Kuppusamy, T. 1987. A parametric model for constitutive properties governing multiphase flow in porous media. *Water Resources Research*, **23**(4): 618-624.
- Parkhurst, D. L. and Appelo, C. A. J. 1999. *User's guide to PHREEQC (Version 2) : a computer program for*

speciation, batch-reaction, one-dimensional transport, and inverse geochemical calculations. Water-Resources Investigations Report 99-4259, USGS.

Peng, D.-Y. and Robinson, D. B. 1976. A new two-constant equation of state. *Industrial and Engineering Chemistry Fundamentals*, **15**(1): 59-64.

Philip, Z. G., Jennings, J. W., Olson, J. E., Laubach, S. E. and Holder, J. 2005. Modeling coupled fracture-matrix fluid flow in geomechanically simulated fracture networks. *Spe Reservoir Evaluation & Engineering*, **8**(4): 300-309.

Pini, R., Storti, G. and Mazzotti, M. 2011. A model for enhanced coal bed methane recovery aimed at carbon dioxide storage. *Adsorption-Journal of the International Adsorption Society*, **17**(5): 889-900.

Poling, B. E., Prausnitz, J. M. and O'Connell, J. P. 2001. *The properties of gases and liquids*, McGraw-hill New York.

Ray, C., Ellsworth, T. R., Valocchi, A. J. and Boast, C. W. 1997. An improved dual porosity model for chemical transport in macroporous soils. *Journal of Hydrology*, **193**(1-4): 270-292.

Robertson, E. P. 2005. Modeling Permeability in Coal Using Sorption-Induced Strain Data. SPE Annual Technical Conference and Exhibition. S. o. P. Engineers. Dallas, Texas.

Robertson, E. P. and Christiansen, R. L. 2008. A permeability model for coal and other fractured, sorptive-elastic media. *SPE Journal*, **13**(3): 314-324.

Ruthven, D. M. 1984. *Principles of adsorption and adsorption processes*. New York, Wiley.

Samardzioska, T. and Popov, V. 2005. Numerical comparison of the equivalent continuum, non-homogeneous and dual porosity models for flow and transport in fractured porous media. *Advances in Water Resources*, **28**(3): 235-255.

Schwartz, R. C., Juo, A. S. R. and McInnes, K. J. 2000. Estimating parameters for a dual-porosity model to describe non-equilibrium, reactive transport in a fine-textured soil. *Journal of Hydrology*, **229**(3-4): 149-167.

Scott, V., Gilfillan, S., Markusson, N., Chalmers, H. and Haszeldine, R. S. 2013. Last chance for carbon capture and storage. *Nature Climate Change*, **3**(2): 105-111.

Sedighi, M., Thomas, H. R., Masum, S. A., Vardon, P. J., Nicholson, D. and Chen, Q., Eds. 2015. Geochemical Modelling of Hydrogen Gas Migration in Unsaturated Bentonite Buffer. Gas Generation and Migration in Deep Geological Radioactive Waste Repositories. London, Geological Society, Special Publications.

Sedighi, M., Thomas, H. R. and Vardon, P. J. 2016. Reactive Transport of Chemicals in Unsaturated Soils: Numerical Model Development and Verification. *Canadian Geotechnical Journal*, **53**(1): 162-172.

Seetharam, S. C., Thomas, H. R. and Cleall, P. J. 2007. Coupled thermo/hydro/chemical/mechanical model for unsaturated soils - numerical algorithm. *International Journal for Numerical Methods in Engineering*, **70**: 1480-1511.

Shi, J. Q. and Durucan, S. 2004. Drawdown induced changes in permeability of coalbeds: A new interpretation of the reservoir response to primary recovery. *Transport in Porous Media*, **56**(1): 1-16.

Shi, J. Q. and Durucan, S. 2005. Gas storage and flow in coalbed reservoirs: Implementation of a bidisperse pore model for gas diffusion in a coal matrix. *Spe Reservoir Evaluation & Engineering*, **8**(2): 169-175.

Šimuněk, J. and van Genuchten, M. T. 2008. Modeling nonequilibrium flow and transport processes using HYDRUS. *Vadose Zone Journal*, **7**(2): 782-797.

Singhal, B. B. S. and Gupta, R. P. 2010. Applied hydrogeology of fractured rocks. Dordrecht, The Netherlands, Springer.

Thararoop, P., Karpyn, Z. T. and Ertekin, T. 2012. Development of a multi-mechanistic, dual-porosity, dual-permeability, numerical flow model for coalbed methane reservoirs. *Journal of Natural Gas Science and Engineering*, **8**: 121-131.

Therrien, R. and Sudicky, E. A. 1996. Three-dimensional analysis of variably-saturated flow and solute transport in discretely-fractured porous media. *Journal of Contaminant Hydrology*, **23**(1-2): 1-44.

Thomas, H. R. and He, Y. 1998. Modelling the behaviour of unsaturated soil using an elasto-plastic constitutive relationship. *Géotechnique*, **48**(5): 589-603.

Thomas, H. R., Sedighi, M. and Vardon, P. J. 2012. Diffusive reactive transport of multicomponent chemicals under coupled thermal, hydraulic, chemical and mechanical conditions. *Geotechnical and Geological Engineering*, **30**(4): 841-857.

Tsang, Y. W. and Pruess, K. 1987. A Study of Thermally Induced Convection near a High-Level Nuclear Waste

- Repository in Partially Saturated Fractured Tuff. *Water Resources Research*, **23**(10): 1958-1966.
- van Genuchten, M. T. 1980. A closed-form equation for predicting the hydraulic conductivity of unsaturated soils. *Soil science society of America journal*, **44**(5): 892-898.
- Ward, C. R. 2002. Analysis and significance of mineral matter in coal seams. *International Journal of Coal Geology*, **50**(1-4): 135-168.
- Warren, J. E. and Root, P. J. 1963. The Behavior of Naturally Fractured Reservoirs. *Society of Petroleum Engineers Journal*, **3**(3): 245-255.
- Wei, Y. S. and Sadus, R. J. 2000. Equations of state for the calculation of fluid-phase equilibria. *Aiche Journal*, **46**(1): 169-196.
- Wu, Y., Liu, J. S., Elsworth, D., Chen, Z. W., Connell, L. and Pan, Z. J. 2010. Dual poroelastic response of a coal seam to CO₂ injection. *International Journal of Greenhouse Gas Control*, **4**(4): 668-678.
- Xu, T. F. and Pruess, K. 2001. Modeling multiphase non-isothermal fluid flow and reactive geochemical transport in variably saturated fractured rocks: 1. Methodology. *American Journal of Science*, **301**(1): 16-33.
- Xu, T. F., Sonnenthal, E., Spycher, N., Pruess, K., Brimhall, G. and Apps, J. 2001. Modeling multiphase non-isothermal fluid flow and reactive geochemical transport in variably saturated fractured rocks: 2. Applications to supergene copper enrichment and hydrothermal flows. *American Journal of Science*, **301**(1): 34-59.
- Zhang, L. and Fredlund, D. 2003. Characteristics of water retention curves for unsaturated fractured rocks. *Proceedings of the 2nd Asian Conference on Unsaturated Soils*, Osaka, Japan.
- Zheng, L. and Samper, J. 2015. Dual-continuum multicomponent reactive transport with nth-order solute transfer terms for structured porous media. *Computational Geosciences*, **19**(4): 709-726.

Tables

Table 1 Material parameters used for verification Test I.

Parameter	Value
Residual volumetric water content,	
Saturated volumetric water content,	
Hydraulic constant, (m^{-1})	
Hydraulic constant, (-)	
Intrinsic permeability, (m^2)	
Absolute viscosity of water, (Pa s)	
Absolute viscosity of gas, (Pa s)	
Density of liquid water, ($kg\ m^{-3}$)	

Table 2 Material parameters used for verification Tests II-a and II-b (Pini, Storti et al. 2011).

Parameter	Value		
Initial porosity, (-)			
Initial permeability, (m ²)			
Sorption rate, (s ⁻¹)			
Poisson's ratio, (-)			
Young's modulus, (Pa)			
Confining pressure, (Pa)			
Coal density, (kg m ⁻³)			
(-)	CH ₄	CO ₂	N ₂
Viscosity, (Pa s)			
(-)			
Langmuir capacity, (mol kg ⁻¹)			
Langmuir constant (sorp.), (Pa ⁻¹)			
Langmuir strain, (-)			
Langmuir constant (swell.), (Pa ⁻¹)			

Table 3 Material parameters used for verification Tests III-a, III-b and III-c.

Material parameter	Relationship / value		
Volumetric weighting factor, (-)			
Degree of water saturation, (-)			
Retardation factor, (-)			
Longitudinal dispersivity, (m)			
	Fracture	Matrix	
Porosity, (-)			
Hydraulic conductivity, (m s ⁻¹)			
Coeff. of mechanical dispersion, (m ² s ⁻¹)			
	Test III-a	Test III-b	Test III-c
Solute mass exchange rates, (s ⁻¹)			

Figures

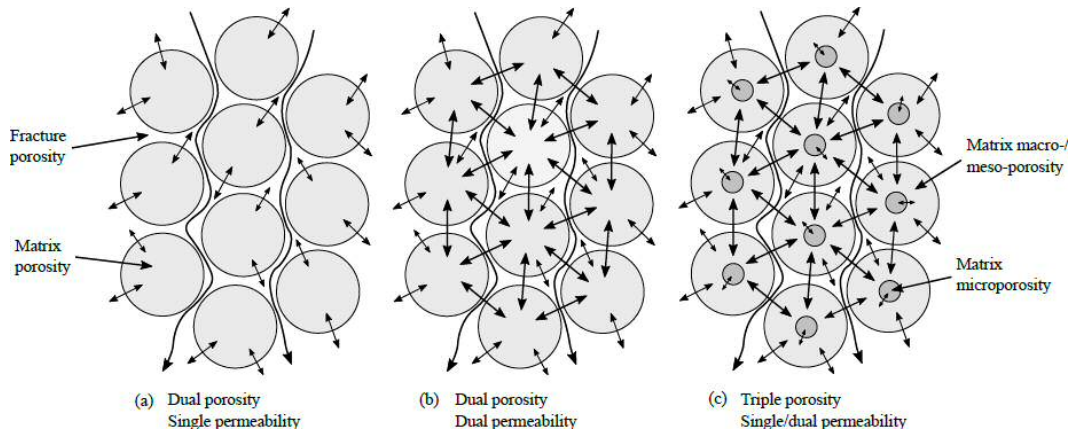


Figure 1 Illustration of the types of dual/triple porosity models (adopted and redrawn from Šimůnek and van Genuchten (2008)). Spheres represent the matrix porosity, including the partition of the macro- and micro-porosity where indicated. Gaps between the spheres represent the fracture porosity. Larger arrows denote permeability pathways and smaller arrows denote inter-porosity mass exchange.

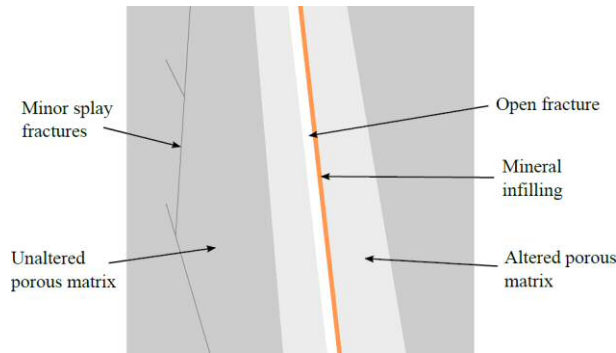


Figure 2 Schematic of a segment of a fractured rock, including open and minor fractures, mineral infillings, unaltered rock matrix, and altered rock matrix (adopted and redrawn from MacQuarrie and Mayer (2005)).

[COLOUR NOT REQUIRED IN FIGURE 2]

Upstream boundary conditions	Initial conditions	Downstream boundary conditions
$0 \leq t \leq 1 \text{ day}$ $Q_g = 0 \text{ mol s}^{-1}$	$T = 298 \text{ K}$ $u_l = -1.8 \times 10^4 \text{ Pa}$ $u_g = RTc_g = 100 \text{ Pa}$	$u_l = 100 \text{ Pa}$ $u_g = RTc_g = 100 \text{ Pa}$ $\frac{\partial u_l}{\partial t} = RT \frac{\partial c_g}{\partial t} = 0.0$
$1 \text{ day} \leq t \leq 11.6 \text{ days}$ Linear increase of Q_g to $1.0 \times 10^{-2} \text{ mol s}^{-1}$		

Figure 3 Schematic of the initial and boundary conditions used for Test I.

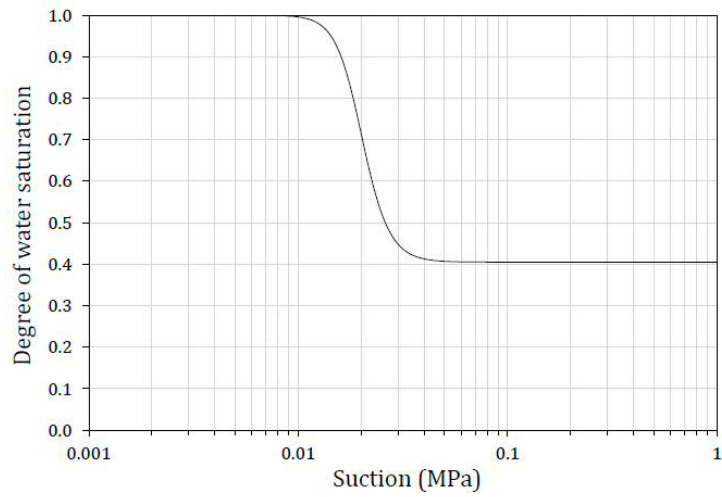


Figure 4 Water retention curve for Test I.

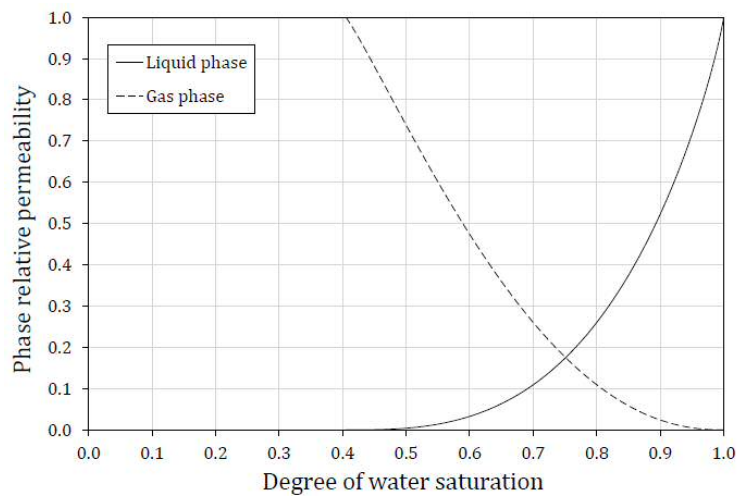


Figure 5 Phase relative permeability curves for Test I.

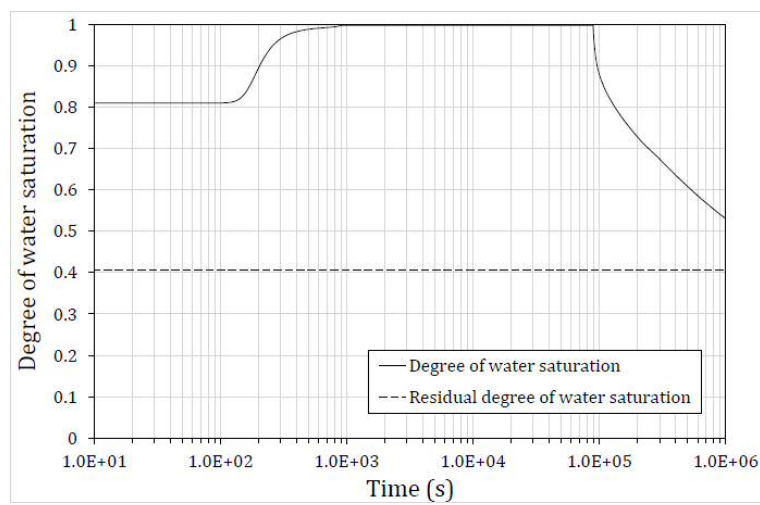


Figure 6 Predicted evolution of the degree of water saturation at the mid-point of the domain (m) for Test I.

Injection boundary conditions	Initial conditions	Production boundary conditions
Test II-a: $c_g^{CO_2} = 1,881.9 \text{ mol m}^{-3}$	Free gas (mol m^{-3}): $c_g^{CO_2} = c_g^{N_2} = 0.0$ $c_g^{CH_4} = 582.4$	$RT \sum_{j=1}^{n_g} c_g^j = 0.1 \times 10^6 \text{ Pa}$ $\sum_{j=1}^{n_g} \frac{\partial c_g^j}{\partial t} = 0.0$
Test II-b: $c_g^{N_2} = 1,522.5 \text{ mol m}^{-3}$	Adsorbed gas (mol kg^{-1}): $s_{gM}^{CO_2} = s_{gM}^{N_2} = 0.0$ $s_{gM}^{CH_4} = 0.75$	

Figure 7 Schematic of the initial and boundary conditions used for Test II-a (CO₂ injection) and Test II-b (N₂ injection).

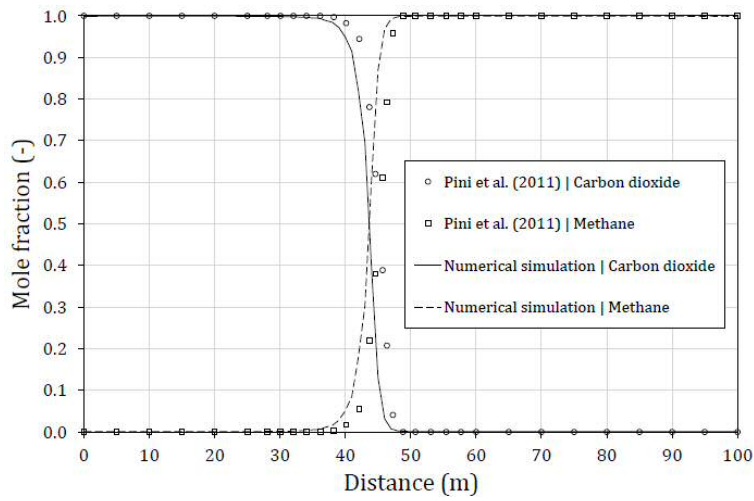


Figure 8 Gas composition of CO₂ and CH₄ (Test II-a) after 42 days compared to Pini et al. (2011).

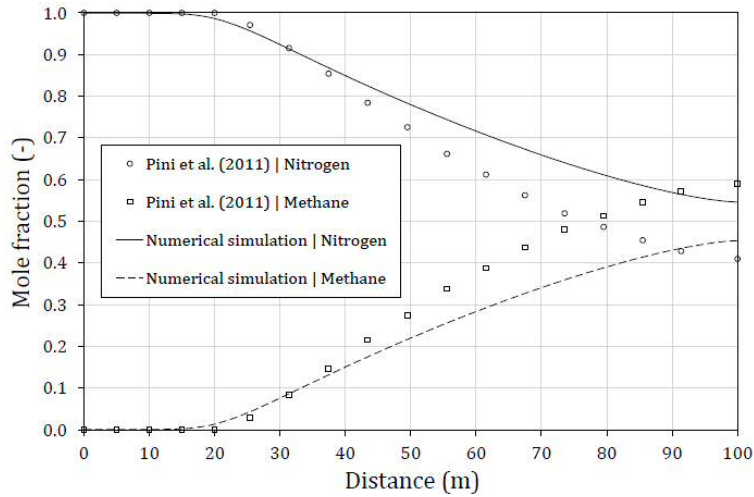


Figure 9 Gas composition of N₂ and CH₄ (Test II-b) after 42 days compared to Pini et al. (2011).

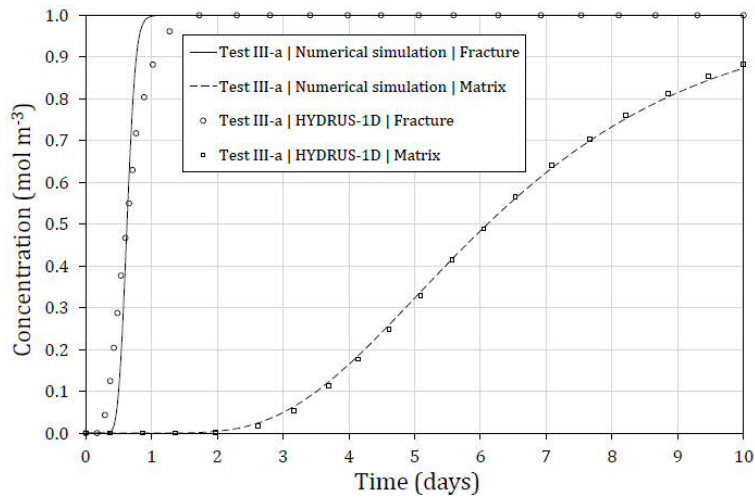


Figure 10 Chemical breakthrough for Test III-a (no mass exchange), obtained using the numerical model and by Šimunek and van Genuchten (2008) using HYDRUS-1D.

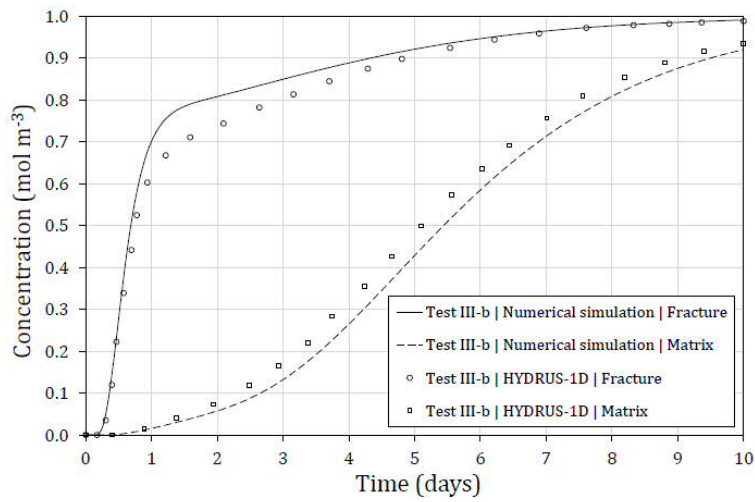


Figure 11 Chemical breakthrough for Test III-b (s-1), obtained using the numerical model and by Šimunek and van Genuchten (2008) using HYDRUS-1D.

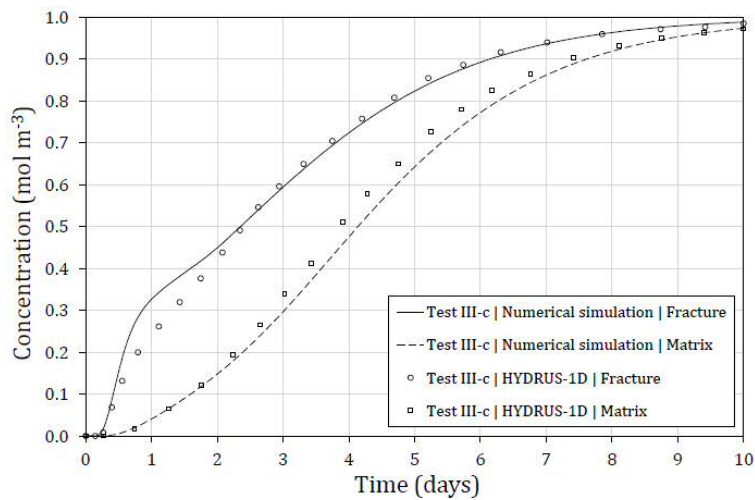


Figure 12 Chemical breakthrough for Test III-c (s-1), obtained using the numerical model and by Šimunek and van Genuchten (2008) using HYDRUS-1D.